

Molecular Cell, Volume 54

Supplemental Information

Single-Molecule Imaging of FtsK Translocation Reveals Mechanistic Features of Protein-Protein Collisions on DNA

Ja Yil Lee, Ilya J. Finkelstein, Lidia K. Arciszewska, David J. Sherratt, and Eric C. Greene

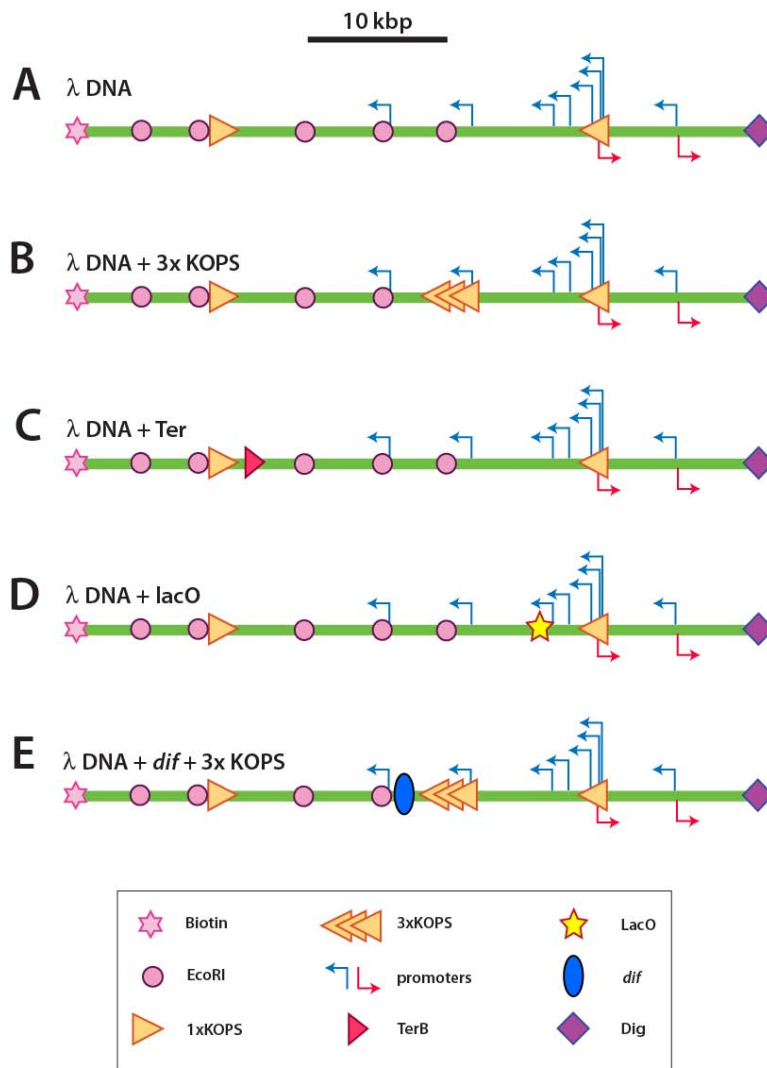


Figure S1, related to all Figures. Schematics of all lambda DNA constructs. (A) Native λ -DNA highlighting the locations of the EcoRI sites, 1x KOPS sites, and the phage promoters. (B) Engineered version of λ -DNA bearing a 3x KOPS site. (C) λ -DNA with a cloned TerB site, (D) λ -DNA with cloned LacO, and (E) λ -DNA with a single *dif* site and a 3x KOPS site. The locations of the biotin and digoxigenin tags are indicated for all DNA constructs.

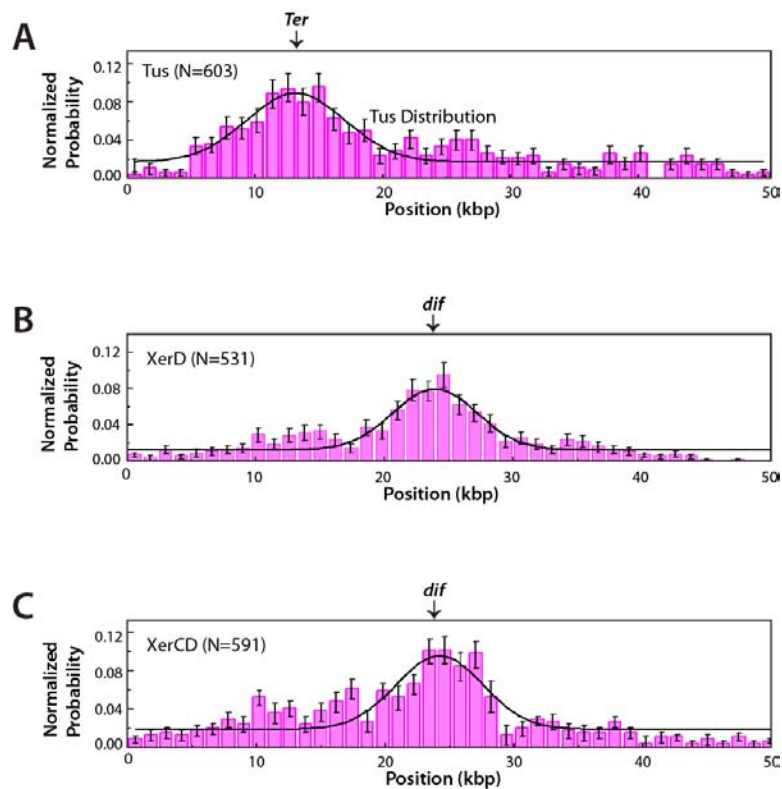


Figure S2, related to Figures 1, 3, and 4. Protein binding distributions. (A) Normalized binding distribution data for Tus on the λ -DNA substrate containing a single Ter site. Normalized binding distribution data for (B) XerD and (C) XerCD collected using a λ -DNA substrate with a single *dif* site. Error bars were generated by Bootstrap analysis of the data, and the black curves represent Gaussian fits to the data (Efron and Tibshirani, 1993; Gorman et al., 2012). Tus, XerD and XerCD all display some degree of nonspecific binding, as revealed in the binding distribution histograms. The broad width of the binding peaks at the cognate target sites results from the DNA being maintained under low tension, which allows for thermal fluctuations of the DNA molecules (also see Lee et al., 2012). Note that we only chose proteins bound to their cognate sites (based on the Gaussian fits to the binding distribution data) for analysis of FtsK collisions.

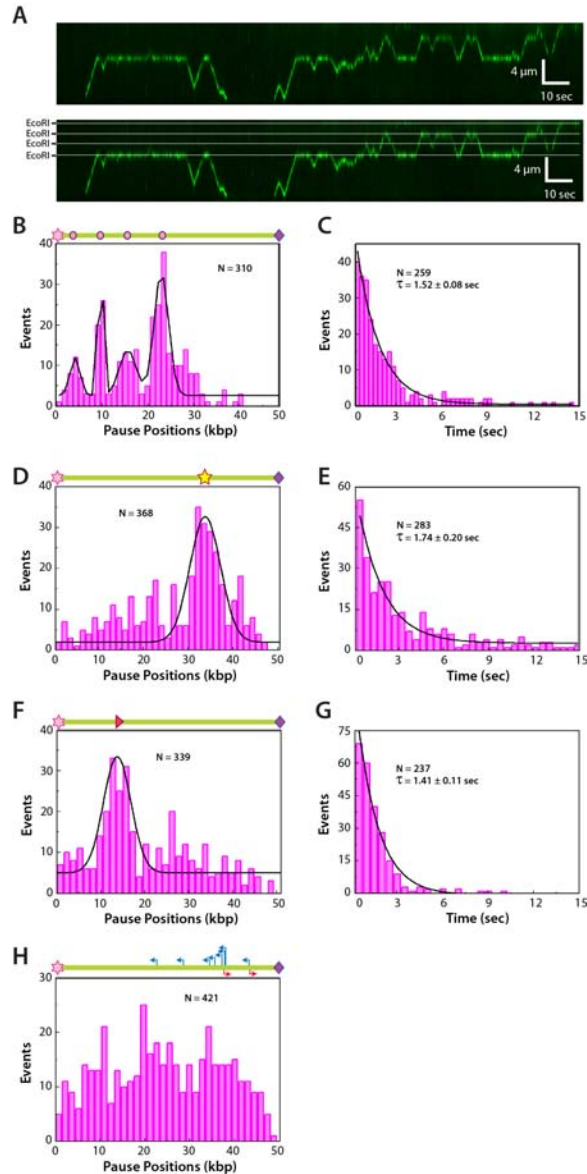


Figure S3, related to Figures 2-4. Collisions between FtsK and unlabeled proteins. (A) Kymographs showing the ATP-dependent translocation of QD-tagged FtsK $\alpha\beta\gamma$ on a λ -DNA substrate with four binding sites for EcoRI and bound by unlabeled EcoRI^{E111Q}. The upper kymograph is not annotated, the same kymograph is shown in the lower panel with annotation indicating the location of the EcoRI binding sites. **(B)** Histogram showing the FtsK $\alpha\beta\gamma$ pause site distributions on DNA bound by unlabeled EcoRI^{E111Q}; the pause site distributions of FtsK are random in the absence of EcoRI^{E111Q} (Lee et al., 2012). **(C)** Pause time distributions for FtsK $\alpha\beta\gamma$ collisions with unlabeled EcoRI^{E111Q}. **(D)** Pause site and **(E)** pause time distributions in the presence of unlabeled Lacl. **(F)** Pause site and **(G)** pause time distributions in the presence of unlabeled Tus. **(H)** Pause site distributions for reactions conducted in the presence of unlabeled RNAP. A schematic of the DNA substrate is shown above each pause site histogram to highlight the location of the binding site(s) for the corresponding roadblock protein; the symbols are the same as in Figure S1.

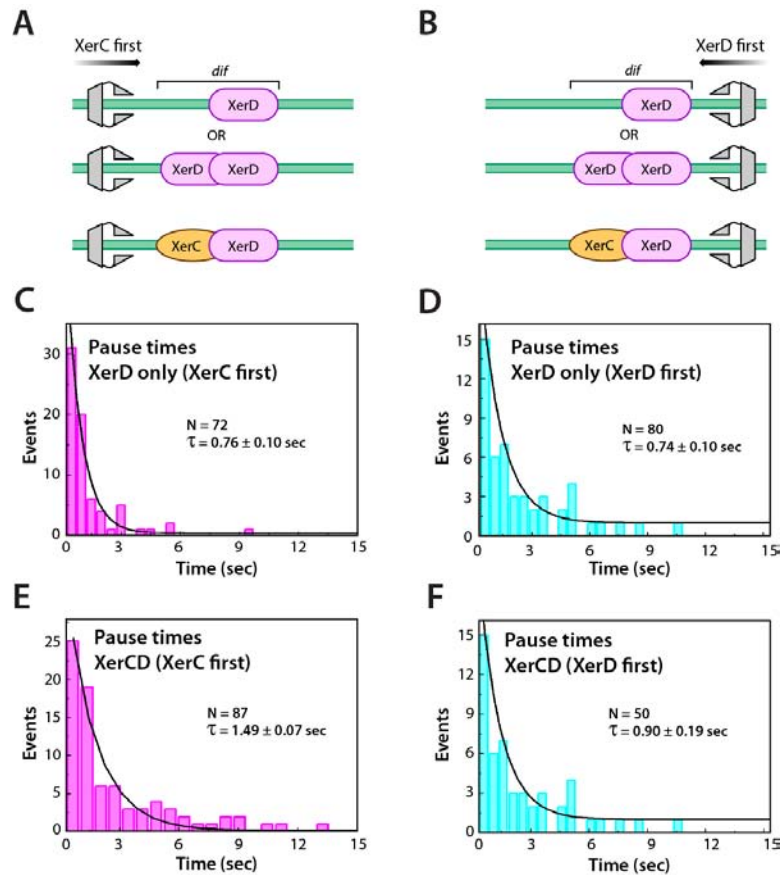


Figure S4, related to Figure 5. FtsK $\alpha\beta\gamma$ collisions with XerD and XerCD. (A) Schematic of XerC-first collisions. **(B)** Schematic of XerD-first collisions. **(C)** FtsK pause times during collisions with XerD in the XerC-first orientation. **(D)** FtsK pause times during collisions with XerD in the XerD-first orientation. **(E)** FtsK pause times during collisions with XerCD in the XerC-first orientation. **(F)** FtsK pause times during collisions with XerCD in the XerD-first orientation.

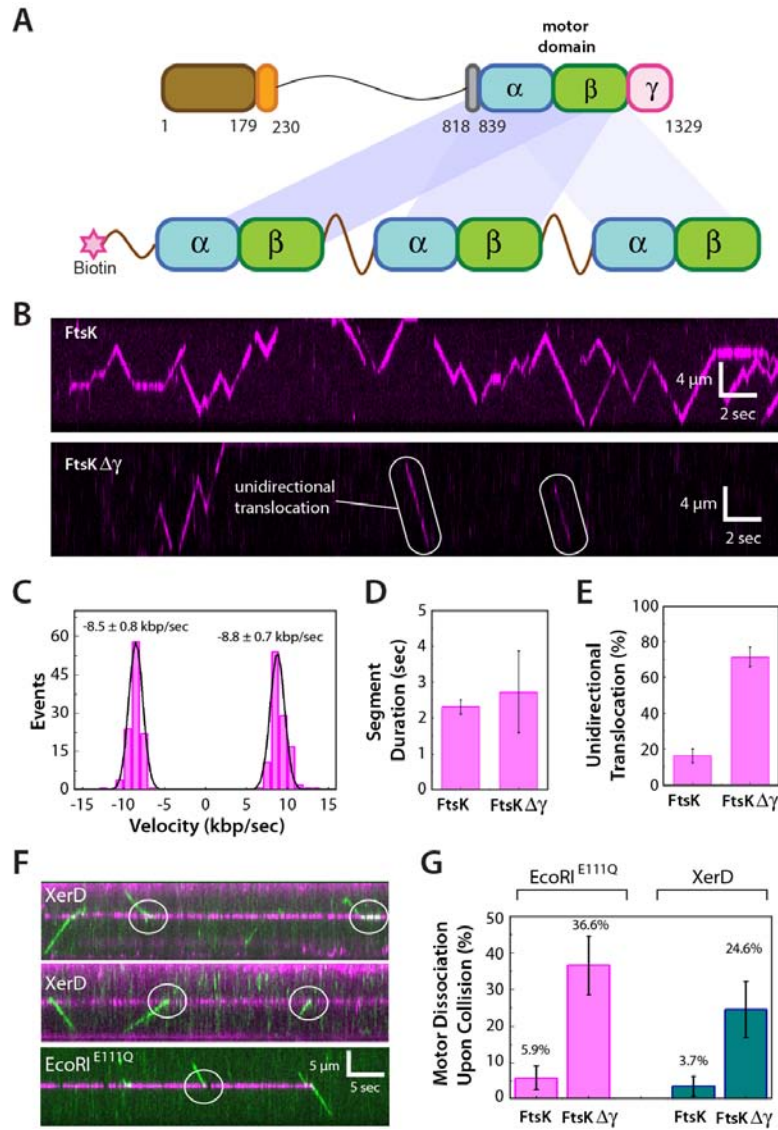


Figure S5, related to Figure 5. DNA translocation properties of FtsKΔγ. (A) Schematic illustration of the FtsKΔγ construct. **(B)** Kymographs comparing the translocation characteristics of FtsKαβγ (upper panel) and FtsKΔγ (lower panel). **(C)** Translocation velocity of FtsKΔγ segregated into the “forward” and “reverse” directions for translocation events going towards the linear barriers or away from the linear barriers respectively (Lee et al., 2012). **(D)** Translocation segment durations for FtsKαβγ and FtsKΔγ. **(E)** Fraction of unidirectional translocation events observed for FtsKαβγ compared to FtsKΔγ. **(F)** Kymographs showing examples of FtsKΔγ collisions with XerD and EcoRI^{E111Q} bound to their respective cognate binding sites. Circles highlight collisions that result in dissociation of FtsKΔγ from the DNA. **(G)** Fraction of collision events that lead to FtsK and FtsKΔγ dissociation upon collision with either EcoRI^{E111Q} or XerD.

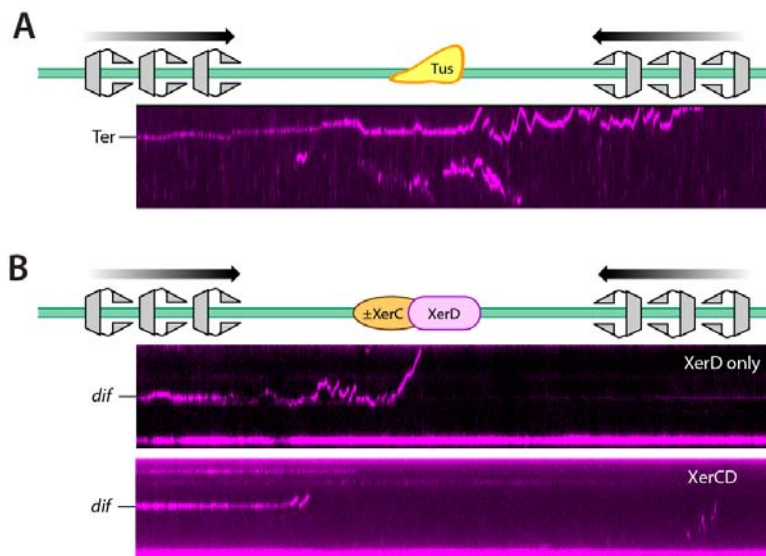


Figure S6, related to Figure 6. Multiple molecules of FtsK can act together to strip Tus, XerD, and XerCD from DNA. (A) Kymograph showing removal of Ter-bound Tus protein (magenta) from DNA by unlabeled molecules of FtsK $\alpha\beta\gamma$. (B) Kymographs showing FtsK $\alpha\beta\gamma$ removal of either XerD (upper panel) or XerCD (lower panel) from DNA.

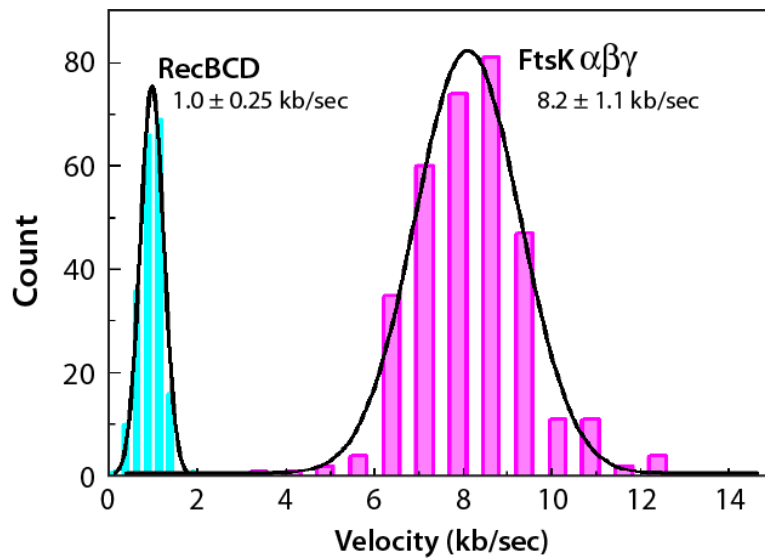


Figure S7, related to Figure 7. Velocity of RecBCD and FtsK $\alpha\beta\gamma$. Histograms showing the translocation velocity distributions of FtsK $\alpha\beta\gamma$ and RecBCD. Data were collected at 27°C in 1 mM ATP under identical buffer conditions.

Table S1, related to Figure 1. DNA oligonucleotides.

Protein	Binding site	Oligonucleotide sequences*
EcoRI ^{E111Q}	EcoRI binding site	5'-GCT AAC CTT AGA GTC ACG AAT TCA AGC CTA CGT CGA AAC G -3'
		5'-CGT TTC GAC GTA GGC TTG AAT TCG TGA CTC TAA GGT TAG C -3'
Lac repressor	Ideal LacO	5'-GCT AAC CTT AAA TTG TGA GCG CTC ACA ATT CGT CGA AAC G -3'
		5'-CGT TTC GAC GAA TTG TGA GCG CTC ACA ATT TAA GGT TAG C -3'
Tus	TerB	5'-GCT AAC CTT AAT AAG TAT GTT GTA ACT AAA GGT CGA AAC G -3'
		5'- CGT TTC GAC CTT TAG TTA CAA CAT ACT TAT TAA GGT TAG C -3'
3xWB-FtsK	3xKOPS	5'-ATC AGG TGC GCA TAA TGT ATA TTA TGT TAA ATC CGA GGG CAG GGC AGG GCA GGG ACG AGT AGT CCA CGC ATT GA-3'
		5'- Cy5 -TCA ATG CGT GGA CTA CTC GTC CCT GCC CTG CCC TGC CCT CGG ATT TAA CAT AAT ATA CAT TAT GCG CAC CTG AT-3'
3xWB-FtsK	1xKOPS	5'-ATC AGG TGC GCA TAA TGT ATA TTA TGT TAA ATC CGA GGG CAG GGA CGA GTA GTC CAC GCA TTG A-3'
		5'- Cy5 -TCA ATG CGT GGA CTA CTC GTC CCT GCC CTC GGA TTT AAC ATA ATA TAC ATT ATG CGC ACC TGA T-3'
RNAP**	PR promoter	5'- Cy3 -GGC CTT GTT GAT CGC GCT TT -3'
		5'- CGT GCG TCC TCA AGC TGC TCT T -3'
XerC/ XerD	dif	5'- Cy5 -GCT AAC GGT GCG CAT AAT GTA TAT TAT GTT AAA TGA AAC G -3'
		5'- CGT TTC ATT TAA CAT AAT ATA CAT TAT GCG CAC CGT TAG C -3'

* The top and bottom strands are both shown, and bold underlined nucleotides represent the binding site for each protein.

** The oligonucleotides for RNAP were used to PCR amplify a 249-bp fragment containing the bacteriophage pR promoter.

Supplemental Experimental Procedures

Proteins & DNA. FtsK $\alpha\beta\gamma$, lac repressor, RNAP and EcoRI^{E111Q} were expressed, purified, and labeled with quantum dots as previously described (Finkelstein et al., 2010; Lee et al., 2012). The linked FtsK $\Delta\gamma$ trimer was constructed using 21 amino acid linkers between each monomer, and was expressed and purified under conditions identical to the full-length linked trimer (Croizat et al., 2010; Lee et al., 2012). The genes for wild type XerC and XerD were cloned into pTXB3 (New England Biolabs), either with or without (as indicated) and C-terminal 3xFLAG tag. XerC and XerD were expressed in BL21(DE3) cells grown in LB (50 $\mu\text{g/ml}$ carbenicillin) at 37°C to an OD₆₀₀ of ~0.6. Cells expressing XerC were cooled to 16°C and induced for ~16 hours by the addition of 0.5 mM IPTG. Cells expressing XerD were induced for ~4 hours at 37°C by the addition of 0.5 mM IPTG. After induction, cells were collected by centrifugation, resuspended in buffer R (50 mM Tris-HCl pH 7.5, 0.1 mM PMSF, 1mM EDTA, 10% sucrose, 0.5 M NaCl), and lysed by sonication. The lysate was clarified by high-speed centrifugation and loaded onto a chitin binding domain column according to the manufacturer suggested protocol (New England Biolabs). Columns were washed with 20 column volumes of buffer W (20 mM Tris-HCl [pH 8.5], 0.5 M NaCl and 1 mM EDTA). The intein-CBD tag was cleaved by flushing the column with buffer W supplemented with 50 mM DTT and 10% glycerol, and incubating overnight at 4 °C. For XerC, peak fractions were pooled, and immediately snap-frozen on liquid N₂ with no further dialysis. For XerD, peak fractions were pooled, dialyzed into storage buffer (50 mM Tris-HCl [pH 8], 0.25M NaCl, 1 mM DTT and 1 mM EDTA), snap-frozen on liquid N₂ and stored at -80°C.

Tus was expressed with an N-terminal strep-tag and a 3xFLAG tag. For expression, cells (*E. coli* JM109) were grown in LB with carbenicillin (50 ng/ml) at 37°C, induced with 1 mM IPTG at OD₆₀₀ of ~0.6, and expressed for 4 hours at 37°C. Cells were harvested by centrifugation and resuspended in lysis buffer (50 mM sodium phosphate [pH 7.5], 100 mM NaCl, 1 mM EDTA, 1 mM DTT, 10% glycerol (w/v), 0.2 mg/ml lysozyme, and 1 mM PMSF), and then stored at -80°C after freezing with liquid N₂. Cells were then thawed and incubated on ice for ~1 hour, and then sonicated. All subsequent steps were carried out at 4°C. After ultracentrifugation, the clarified lysate was precipitated with 40% ammonium sulfate, and the resulting protein pellets were resuspended in buffer containing 50 mM sodium phosphate [pH 7.5], 100 mM NaCl, 1 mM EDTA, 1 mM DTT, and 20% glycerol. The resuspended proteins were then applied to a Strep-Tactin column (IBA Lifesciences) by gravity flow, washed with 5 column volumes of buffer containing 50 mM Tris-HCl [pH 7.5], 100 mM NaCl, 1 mM EDTA, 20% glycerol (w/v), and 1 mM DTT. Tus was eluted with buffer containing 50 mM Tris-HCl [pH 7.5], 100 mM NaCl, 1 mM EDTA, 2.5 mM d-desthiobiotin (Sigma-Aldrich), 20% glycerol, and 2 mM DTT. The fractions containing Tus were pooled and dialyzed against storage buffer (50 mM Tris [pH 7.5], 100 mM NaCl, 1 mM EDTA, 20% glycerol (w/v), and 1 mM DTT). Purified fractions were frozen with liquid N₂ and stored at -80°C.

DNA curtains. Double-tethered curtains were made as described (Gorman et al., 2010; Greene et al., 2010). In brief, after deposition of the bilayer, the sample chamber was flushed with buffer A (10 mM Tris-HCl [pH 8.0] and 100 mM NaCl) containing 30 $\mu\text{g ml}^{-1}$ of anti-DIG Fab (Roche Cat. No. 1214667001) and then incubated for 20 minutes to allow the Fab fragments to adsorb to the pentagons. The chamber was then flushed with buffer B (40 mM Tris-HCl [pH 8.0], 50 mM NaCl, and 2 mM MgCl₂) for 5 minutes. Streptavidin (0.02 mg ml⁻¹) in buffer B was then injected

into the sample chamber and incubated for 20 minutes. After rinsing with additional buffer B, λ -DNA (15-20 pM) labeled at one end with biotin and at the other end with digoxigenin (DIG) (Lee et al., 2012), was injected, incubated for 10 minutes, and unbound DNA was removed by flushing with buffer at 0.3 ml min^{-1} . Application of flow aligned the DNA molecules along the diffusion barriers, and stretched the molecules so the free ends could attach to the pentagons.

Dissociation equilibrium constant measurements.

Nitrocellulose filter binding assays. Filter binding assays were used to measure the K_d values for EcoRI^{E111Q}, lac repressor, and Tus. DNA oligonucleotides containing single binding site for each protein were synthesized (IDT) as shown in Supplementary Table S1. The oligonucleotides were labeled using T4 polynucleotide kinase (NEB) and γ [P^{32}]-ATP (PerkinElmer). Labeling reactions were stopped with EDTA. The two complementary oligonucleotides were annealed by heating the mixture to 95°C and cooling slowly. The DNA was then extracted with phenol:chloroform, and purified with spin-column (Centri-Spin-20, Princeton Separations). For the binding assay, nitrocellulose filters (HAWP02500, 0.45 μm HA, Millipore) were pre-soaked in binding buffer (40 mM Tris-HCl [8.0], 50 mM NaCl, 2 mM MgCl_2 , 2 mM DTT) for at least 1 hour before use. A fixed concentration of ^{32}P -labeled DNA (0.5 pM) was incubated with varying amounts of the protein of interest in reaction buffer containing 40 mM Tris-HCl [8.0], 50 mM NaCl, 2 mM MgCl_2 , 2 mM DTT, and 0.2 mg/ml BSA at 27°C for 30 min. Samples were loaded onto the nitrocellulose filter through a vacuum filtration manifold. Filters were then washed with 5 volumes of reaction buffer. The nitrocellulose filters were then dried at 60°C , and the amount of radioactive DNA bound to the filters was measured by scintillation counter (LS-6500, Beckton-Dickinson). Each experimental data point was repeated in triplicate.

Gel shift assays. Gel shift assays were used to measure the K_d values for RNAP, FtsK^{D1121A}, XerD, and XerCD. Reactions with RNAP utilized a Cy3-labeled PCR fragment of the λ P_R -promoter, essentially as described. The PCR product was purified with spin column (Qiagen). Reactions with FtsKD1121A, XerD, and XerCD used synthetic oligonucleotides labeled with Cy5 (Table S1). In each case the DNA (300 pM) was incubated with different concentrations of protein in reaction buffer containing 40 mM Tris-HCl [8.0], 50 mM NaCl, 2 mM MgCl_2 , 2 mM DTT, and 0.2 mg/ml BSA at 27°C for 30 min. Reactions with FtsK^{D1121A} were supplemented with 1 mM ATP. Samples were then resolved on 4-5% non-denaturing polyacrylamide gel for 1 hour at 4°C ; for experiments with FtsK^{D1121A} the gel and running buffers with supplemented with 1 mM ATP. The Cy3 or Cy5 fluorescence was then quantitated with a Typhoon variable mode laser scanner (GE Healthcare). All reactions were repeated in triplicate.

Dissociation rate measurements.

DNA curtain experiments. The dissociation rate (k_{off}) is an inverse of protein lifetime on its binding site. The dissociation rates of RNAP, 3xWB FtsK^{D1121A}, XerD, and XerCD were obtained by measuring the lifetimes using double-tethered DNA curtain experiments. For RNA polymerase, QD-tagged RNAP was injected into flowcell and bound promoter sites in RNAP reaction buffer containing 40 mM Tris-HCl [8.0], 10 mM KCl, 1 mM MgCl_2 , 0.2 mg/ml BSA, and 2 mM DTT supplemented with 1 mM biotin. Free QDs were washed away, the buffer was

switched into the FtsK collision buffer (40 mM Tris-HCl [8.0], 50 mM NaCl, 2 mM MgCl₂, 0.2 mg/ml BSA, 2 mM DTT, 1 mM ATP, plus 1 mM biotin. Measurements were carried out over a period of 1-hour and 100-msec images were collected at 2-second intervals with laser shuttering in between data acquisition. The average lifetime of RNAP was then calculated as previously described (Wang et al., 2013). Briefly, for the promoter-binding RNAPs, I collected the dissociation time intervals $\{t_{(1)}, t_{(2)}, \dots, t_{(N)}\}$, where N is the total number of molecules. The set was sorted into ascending order: $\{t_{(1)} \leq t_{(2)} \leq \dots \leq t_{(N)}\}$. The residual dissociation times between events were then calculated as $N_m = t_{(m+1)} - t_{(m)}$ and a corrected time for each measured event was determined as $t_{c(m)} = N_m * (N - m)$. The lifetime was determined by averaging the $\{t_{c(m)}\}$, and the dissociation rate was obtained as the inverse of the lifetime. The dissociation rates for FstK^{D1121A}, XerD, and XerCD were calculated using the same methodology, with the following exceptions. The FstK^{D1121A} experiments used the DNA substrates bearing the 1x and 3x KOPS sequences (Figure S1) and the data were segregated for each of the different sites. Experiments with XerD and XerCD utilized a DNA substrate containing a dif site, and XerD and XerCD were labeled with anti-FLAG QDs.

Filter-binding assays. The dissociation rates (k_{off}) for EcoRI^{E111Q}, lac repressor, and Tus were obtained by nitrocellulose filter binding assays. DNA curtains could not be used to measure the dissociation rates for these proteins because they bind DNA so tightly that their binding lifetimes exceeded the binding lifetimes of the QD tags (not shown). The basic protocol is the same as described above for the nitrocellulose filter-binding assay used for Kd measurements, with the following modifications. For the dissociation rate measurements, 1 nM of target protein was incubated with 10 pM of ³²P labeled oligonucleotide in binding buffer containing 40 mM Tris-HCl [8.0], 50 mM NaCl, 2 mM MgCl₂, and 2 mM DTT for 40 min. The reactions were then challenged by the addition of a large molar excess unlabeled competitor oligonucleotide (10 nM). The filter-binding assay for each sample was then carried out as a function of time. The lifetime of proteins was obtained by fitting the bound fraction according to time with a single exponential function, and the dissociation rate was calculated as the inverse of the lifetime. All experiments were performed in triplicate.

Supplemental Video Legends

Supplemental Video S1, related to Figure 1. Wide-field image of FtsK $\alpha\beta\gamma$ translocation on a double-tethered DNA curtain. This video shows a typical field of view for an experiment with FtsK $\alpha\beta\gamma$ bound to a double-tethered DNA curtain. FtsK $\alpha\beta\gamma$ is shown in green, and the blinking fluorescence signals confirm the presence of single QDs. The DNA is not labeled because previous studies have shown that intercalating dyes inhibit the DNA translocation activity of FtsK. Variations in signal intensity arise from inherent heterogeneity of the intensities of individual QDs, differences in the number of QDs per hexamer (one vs. two), and occasional collisions between FtsK hexamers giving rise to larger FtsK oligomers.

Supplemental Video S2, related to Figure 1. FtsK $\alpha\beta\gamma$ translocation along a single DNA molecule. This video shows a single DNA molecule bound by one FtsK $\alpha\beta\gamma$ motor complex. The graph to the right shows the position of the QD-tagged FtsK $\alpha\beta\gamma$ over time, and gaps in the tracking data correspond to QD blinking.

Supplemental Video S3, related to Figure 7. DNA molecule bound by multiple FtsK $\alpha\beta\gamma$ motors. This video shows one double-tethered DNA molecule bound by multiple motors, reflecting the typical binding density for experiments conducted at 5 pM FtsK $\alpha\beta\gamma$. The graph to the right shows the position of the QD-tagged FtsK $\alpha\beta\gamma$ over time, and gaps in the tracking data correspond to both QD blinking and the inability to track closely spaced trajectories on the same DNA molecule.

Supplemental Video S4, related to Figure 7. Head-on collision between FtsK $\alpha\beta\gamma$ and RecBCD. This video shows a single-tethered DNA molecule bound by both FtsK $\alpha\beta\gamma$ (green) and RecBCD (magenta). RecBCD is bound at the free end of the DNA, and FtsK $\alpha\beta\gamma$ starts out bound to a 3x KOPS site. Translocation is initiated by the injection of 1 mM ATP, and the graph to the right tracks the positions of both proteins over time.

Supplemental References

Crozat, E., Meglio, A., Allemand, J., Chivers, C., Howarth, M., Vènién-Bryan, C., Grainge, I., and Sherratt, D. (2010). Separating speed and ability to displace roadblocks during DNA translocation by FtsK. *EMBO J* 29, 1423 - 1433.

Efron, B., and Tibshirani, R. (1993). *An Introduction to the Bootstrap* (New York, Chapman and Hall, Inc.).

Finkelstein, I., Visnapuu, M., and Greene, E. (2010). Single-molecule imaging reveals mechanisms of protein disruption by a DNA translocase. *Nature* 468, 983 - 987.

Gorman, J., Fazio, T., Wang, F., Wind, S., and Greene, E. (2010). Nanofabricated racks of aligned and anchored DNA substrates for single-molecule imaging. *Langmuir* 26, 1372 - 1379.

Gorman, J., Wang, F., Redding, S., Plys, A.J., Fazio, T., Wind, S., Alani, E.E., and Greene, E.C. (2012). Single-molecule imaging reveals target-search mechanisms during DNA mismatch repair. *Proc Natl Acad Sci U S A* 109, E3074-3083.

Greene, E., Wind, S., Fazio, T., Gorman, J., and Visnapuu, M. (2010). DNA curtains for high-throughput single-molecule optical imaging. *Methods Enzymol* 472, 293 - 315.

Lee, J.Y., Finkelstein, I.J., Crozat, E., Sherratt, D.J., and Greene, E.C. (2012). Single-molecule imaging of DNA curtains reveals mechanisms of KOPS sequence targeting by the DNA translocase FtsK. *Proc Natl Acad Sci U S A* 109, 6531-6536.

Wang, F., Redding, S., Finkelstein, I.J., Gorman, J., Reichman, D.R., and Greene, E.C. (2013). The promoter-search mechanism of *Escherichia coli* RNA polymerase is dominated by three-dimensional diffusion. *Nat Struct Mol Biol* 20, 174-181.